ELSEVIER

Biophysical Chemistry 98 (2002) 149–164

Biophysical Chemistry

www.elsevier.com/locate/bpc

A tertiary two-state allosteric model for hemoglobin☆

Eric R. Henry, Stefano Bettati[1], James Hofrichter, William A. Eaton*

Laboratory of Chemical Physics, Building 5, National Institute of Diabetes, Digestive and Kidney Diseases, National Institutes of Health, Bethesda, MD 20892-0520, USA

Received 29 October 2001; received in revised form 26 December 2001; accepted 26 December 2001

Abstract

The two-state allosteric model of Monod, Wyman, and Changeux (MWC) provides an excellent description of homotropic effects in a vast array of equilibrium and kinetic measurements on cooperative ligand binding by hemoglobin. However, in contrast to experimental observations, the model does not allow for alteration of the ligand affinity of the *T* quaternary structure by allosteric effectors. This failure to explain heterotropic effects has been appreciated for over 30 years, and it has been generally assumed to result from tertiary conformational changes in the absence of a quaternary change. Here we explore a model that preserves the essential MWC idea that binding without a quaternary conformational change is non-cooperative, but where tertiary conformations of individual subunits play the primary role instead of the quaternary conformations. In this model, which we call the 'tertiary two-state (TTS) model', the two affinity states correspond to two tertiary conformations of individual subunits rather than the two quaternary conformations of the MWC two-state allosteric model. Ligation and the *R* quaternary structure bias the subunit population toward the high affinity tertiary conformation, while deligation and the *T* quaternary structure favor the low affinity tertiary conformation. We show that the model is successful in quantitatively explaining a demanding set of kinetic data from nanosecond carbon monoxide photodissociation experiments at times longer than ~ 1 μs. Better agreement between the model and the submicrosecond kinetic data may result from detailed considerations of the distribution and dynamics of conformational substates of the two tertiary conformations. The model is consistent with the results of solution, gel, and single crystal oxygen binding studies, but underestimates the population of doubly-liganded molecules determined in low-temperature electrophoresis experiments.

Keywords: Allostery; Hemoglobin; Quaternary structure; Oxygen binding; Cooperative binding; Conformational kinetics; Conformational substates; Stretched exponential kinetics

☆ Dedicated to Maurizio Brunori.

*Corresponding author. Tel.: +1-301-496-6030; fax: +1-301-496-0825.

E-mail address: eaton@helix.nih.gov (W.A. Eaton).

[1] Present address. Department of Biochemistry and Molecular Biology, Institute of Physical Sciences, and Italian National Institute for the Physics of Matter, University of Parma, 43100 Parma, Italy.

0301-4622/02/$ - see front matter
PII: S0301-4622(02)00091-1

1. Introduction

It is a great pleasure to be able to contribute this article in honor of Maurizio Brunori. The article is concerned with the mechanism of oxygen binding to hemoglobin, the paradigm for understanding cooperative effects in multi-subunit proteins. Brunori and the Rome group have been at the center of experimental and conceptual developments of this subject for over 40 years. For this special issue, it seemed only fitting to focus on an aspect of hemoglobin research that has always been of great interest to Brunori, namely the two-state allosteric model of Monod, Wyman, and Changeux (MWC) [1,2]. Jeffries Wyman was a mentor, and friend of Brunori and a colleague in the biochemistry department at 'La Sapienza' from 1961 to 1986 [2]. Moreover, as explained below, Brunori and colleagues are responsible for an important extension of this model.

The MWC model [1] has provided a powerful framework for investigating the mechanism of cooperativity in hemoglobin [3–11] and many other multi-subunit proteins [12]. In its simplest form, the MWC partition function for hemoglobin is:

$$\Xi = L(1+K_T p)^4 + (1+K_R p)^4 \quad (1)$$

where L is the population ratio of fully deoxygenated T and R quaternary structures, K_T is the oxygen affinity in the T quaternary structure, K_R is the oxygen affinity in the R quaternary structure, and p is the oxygen pressure. This partition function requires the four subunits to be structurally identical (i.e. the molecule must possess either tetrahedral or square symmetry), and therefore cannot be strictly correct for hemoglobin. Two modifications of the MWC model address this problem. The first takes into account the chemical inequivalence of α and β subunits [8]:

$$\Xi = L(1+K_T^{\alpha} p)^2(1+K_T^{\beta} p)^2 + (1+K_R^{\alpha} p)^2(1+K_R^{\beta} p)^2 \quad (2)$$

This partition function retains the essential idea contained in Eq. (1) that binding without a change in quaternary structure is non-cooperative and that all cooperativity arises from a shift in the population from the low affinity T quaternary structure to the high affinity R quaternary structure as the oxygen pressure increases. The second modification is an extension of the MWC model by Brunori and co-workers, which they called the dimeric cooperon model [13,14]. This model retains the MWC symmetry assumption implicit in Eq. (1) that there is no cooperative interaction in either quaternary structure between structurally identical units, the so-called 'protomers' of MWC, but allows for cooperative interaction within the protomers. In the case of hemoglobin the protomers are the αβ dimers that are interchanged by the twofold rotation axis, y (Fig. 1). The modification of Eq. (2) by Brunori and co-workers derives from the partition function:

$$\Xi = L\{1+(K_T^{\alpha 1}+K_T^{\beta 1})p+\delta_T^{\alpha 1\beta 1}K_T^{\alpha 1}K_T^{\beta 1}p^2\}\{1+(K_T^{\alpha 2}+K_T^{\beta 2})p+\delta_T^{\alpha 2\beta 2}K_T^{\alpha 2}K_T^{\beta 2}p^2\} + \{1+(K_R^{\alpha 1}+K_R^{\beta 1})p+\delta_R^{\alpha 1\beta 1}K_R^{\alpha 1}K_R^{\beta 1}p^2\}\{1+(K_R^{\alpha 2}+K_R^{\beta 2})p+\delta_R^{\alpha 2\beta 2}K_R^{\alpha 2}K_R^{\beta 2}p^2\} \quad (3)$$

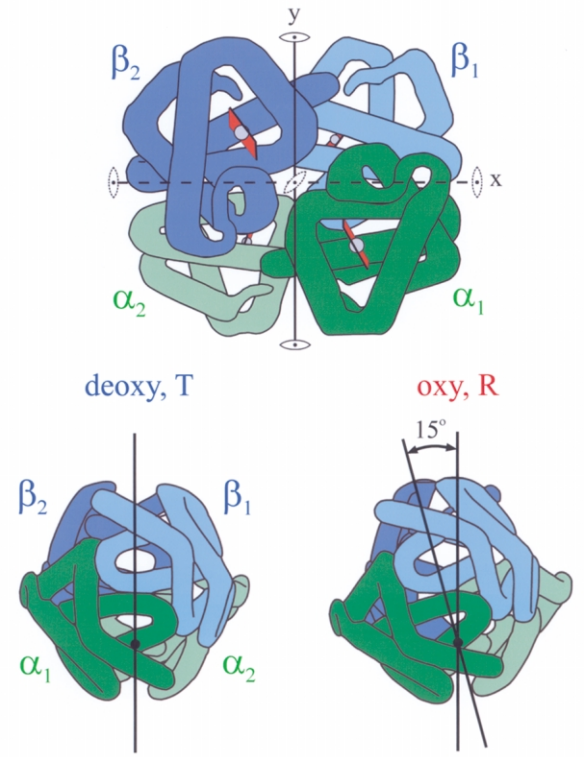

Fig. 1. Schematic structure of hemoglobin. Adapted from Dickerson and Geis [48].

In this partition function the $\alpha 1\beta 1$ and $\alpha 2\beta 2$ dimers are the two protomers of MWC (the function is written out in detail to anticipate the importance of the equivalence of the two $\alpha\beta$ dimers). There is a cooperative interaction of magnitude δ between α and β subunits on the same dimer without a change in quaternary structure, but no interaction across the dimer interface, i.e. between protomers. In other words, the second ligand binds to an $\alpha\beta$ dimer in a fixed quaternary structure with an affinity that is δ-fold higher than the first ligand, instead of with its intrinsic affinity as required by Eq. (2); however, binding either the first or second ligand to one dimer has no effect on the ligand affinity of the other dimer.

Brunori and co-workers assumed that cooperative binding could occur in the *T* quaternary structure ($\delta_T > 1$), but not in *R* ($\delta_R = 1$). They also assumed that the α and β subunits in *R* have equal affinities. Since the twofold symmetry axis makes $\alpha 1$ equivalent to $\alpha 2$ and $\beta 1$ equivalent to $\beta 2$, Eq. (3) simplifies to the partition function for the dimeric cooperon model [14]:

$$\Xi = L\{1 + (K_T^{\alpha} + K_T^{\beta})p + \delta_T K_T^{\alpha} K_T^{\beta} p^2\}^2 + \{1 + K_R p\}^4 \quad (4)$$

Brunori and co-workers showed that thermodynamic linkage requires cooperative oxygen binding to *T* state $\alpha\beta$ dimers to result in a quaternary equilibrium constant and a tetramer–dimer dissociation constant that are position-dependent for *T*-state tetramers with one α and one β subunit liganded, i.e. the constants for $(\alpha 1O_2\beta 1O_2)(\alpha 2\beta 2)$ and $(\alpha 1O_2\beta 1)(\alpha 2\beta 2O_2)$ cannot be the same. They further showed that using this partition function, the (currently) observed pattern of the ratios of tetramer–dimer dissociation constants [15] could be reproduced [14].

A value of δ_T has been estimated from two different kinds of experiments. From single crystal studies of oxygen binding to the *T* quaternary structure the Hill *n* was found to be 1.0, suggesting perfectly non-cooperative binding [16–18]. However, after correcting for the difference in the intrinsic affinity of α and β subunits, cooperative binding to *T* is exposed (Hill $n < 1.2$), corresponding to $1 < \delta_T < 2.5$ [17,18]. The more extensive series of experiments was the determination of the tetramer–dimer dissociation constants for the 10 distinct ligation microstates [15]. These data are consistent with a comparably small value of $\delta_T \approx 4$ [10]. Most recently, an innovative measurement of the tetramer–dimer dissociation rate of a rapidly prepared doubly liganded hybrid also demonstrates that the position-dependence and therefore δ_T must be small [19]. Although it appears that there is cooperativity in binding within the *T* quaternary structure, it is small compared to the increase in affinity of $\sim 10^3$-fold generated by the change in quaternary structure from *T* to *R*. The net result, then, of the analysis of equilibrium data is that a change in quaternary structure is primarily responsible for cooperativity, as postulated by MWC, and that the deviation from perfect MWC (Eqs. (1) and (2)) can be quantitatively accounted for by the dimeric cooperon model of Brunori and co-workers [10]. Their model allows for cooperative interaction within $\alpha\beta$ dimers, but does not abandon the MWC symmetry assumption of no cooperative interaction between $\alpha\beta$ dimers.

Kinetics provide a more demanding test of a model in cooperative systems because intermediates are present at much higher concentrations than at equilibrium. Several studies have shown that the rather complex kinetics of hemoglobin are also consistent with the MWC model of Eq. (1). This was first qualitatively demonstrated for ligand dissociation and bimolecular rebinding kinetics by Hopfield, Shulman and Ogawa using the results of Gibson, Antonini, and Brunori [4,7,20]. Subsequently, Sawicki and Gibson [21] investigated the kinetics following microsecond photodissociation of the carbon monoxide complex, and concluded that the MWC model was not consistent with the data. More recently, however, Henry et al. [22] reinvestigated these kinetics with the improved time resolution of nanosecond lasers. They showed that the multiphasic kinetics of both ligand rebinding and conformational changes in the nanosecond–millisecond time regime could be explained with a kinetic version of the MWC model described by the partition functions in Eqs. (1) and (2) that was extended to include geminate rebinding and tertiary conformational relaxation in the *R* state [22]. The agreement between the model

and the data is excellent, again suggesting that cooperativity in the *T* quaternary structure is small.

A remaining issue, which is the subject of this paper, is whether the kinetic data are also consistent with models that address a long-known deficiency in the MWC model, namely the role of tertiary conformational changes observed to occur, e.g. upon ligand binding, without a change in quaternary structure [3,9,23,24]. According to MWC, all conformational changes are associated with the change in quaternary structure. For this reason the MWC model fails to explain heterotropic effects, such as the decrease in oxygen affinity of the *T* quaternary structure with decreasing pH [25–27]. In the MWC model allosteric effectors alter oxygen affinity only by preferentially binding to the *T* quaternary structure, without altering K_T. The importance of purely tertiary conformational changes for explaining heterotropic effects was recognized in early statistical mechanical models motivated by Perutz's stereochemical mechanism [3,5,6]. In particular, in the Szabo and Karplus model tertiary conformational changes, which accompany oxygen binding in the *T* quaternary structure and rupture salt bridges, explain the change in K_T with pH [5,28]. We should note, however, that breaking salt bridges in accord with the Perutz stereochemical mechanism is a conformational change that has yet to be directly observed [11].

Herzfeld and Stanley [6] proposed a more general model, which allows for tertiary conformational changes without ligand binding, cooperative interactions without a change in quaternary structure, and considers both tertiary and quaternary heterotropic effects. The Pauling sequential model [29,30], now of only historical interest for hemoglobin studies, and the MWC model are limiting cases. Another interesting limiting case is one in which there are no cooperative interactions within a quaternary structure, as in the MWC model, but tertiary–quaternary coupling is incomplete. That is, high and low affinity conformations of individual subunits, which we shall call *r* and *t*, exist in equilibrium within each quaternary structure. In this model the affinity state corresponds to the tertiary conformation of the subunit, not the quaternary structure. The quaternary structure influences the affinity by biasing the $t \rightleftharpoons r$ conformational equilibrium, the *T* conformation favoring *t* and the *R* conformation favoring *r*. In both *R* and *T* ligand binding favors *r*. As we shall see, the net result is that while liganded subunits in *R* are all in the *r* conformation and unliganded subunits in *T* are all in the *t* conformation, both *r* and *t* conformations are significantly populated at equilibrium in unliganded subunits in *R* and liganded subunits in *T*. We shall call this model the tertiary two-state allosteric (TTS) model, to distinguish it from the classical, quaternary two-state allosteric (QTS) model of MWC. The partition function for this model with equal α and β affinities is:

$$\Xi = \frac{L'}{l_T^4}\{1 + K_r p + l_T(1 + K_t p)\}^4 + \{1 + K_r p + l_R(1 + K_t p)\}^4 \quad (5)$$

where L' is the ratio of the *T* to *R* populations in which all the subunits of *T* are unliganded *t* and all the subunits of *R* are unliganded *r*, l_T is the ratio of *t* to *r* populations of the unliganded subunits in the *T* quaternary structure, l_R is the corresponding equilibrium constant in the *R* quaternary structure, and K_t and K_r are the affinities of the subunits in the *t* and *r* conformations in which the liganded subunits remain in *t* and *r*, respectively. In this model, heterotropic effectors can influence L', l_R, and l_T, but not K_r or K_t. In the limit where l_T is large and l_R small, Eq. (5) is identical to the QTS partition function (Eq. (1)) with $L = L'$, $K_T = K_t$ and $K_R = K_r$. Notice that the mathematical form of the partition functions in Eqs. (1) and (5) are the same, and therefore provide identical fits to equilibrium oxygen binding data. However, the structural interpretation of the parameters is different because tertiary and quaternary conformations are now considered separately, rather than as the concerted conformational change of the QTS model of MWC.

Our consideration of the TTS allosteric model has been motivated by its simplicity and intuitively appealing way of considering the relative roles of tertiary and quaternary conformations. In addition to explaining the condition dependence of the affinity for the first ligand (K_T of MWC), it

provides a conceptual framework for describing the complex conformational kinetics of hemoglobin, as well as several important experimental observations on molecules constrained to remain in the *T* quaternary structure. First, the affinity of single crystals of *T*-state hemoglobin was found to be lower than the *T* state in solution and independent of pH [16,17]. This result was explained by suggesting that the extreme low affinity results from suppression by lattice contacts not only of the $T \rightarrow R$ quaternary conformational change, but also of the tertiary conformational change that is presumed to occur in solution and is responsible for the (tertiary) Bohr effect [17]. The crystal binding affinity would correspond to K_t in the TTS allosteric model. Another intriguing observation has been that the Hill *n* for oxygen binding to hemoglobin trapped in the *T* state in silica gels is much less than 1.0, indicating heterogeneous binding within *T* [31,32]. The proposed explanation is that the constraints of the gel not only prevent the *T* to *R* quaternary conformational change but also prevent interconversion of tertiary structures having different affinities within *T* [33,34]. Interestingly, the lower affinity state in the gel has the same affinity as the crystal [34]. Finally, spectroscopic studies have suggested that there are only two tertiary conformations. Time-resolved absorption spectra following photodissociation of the carbon monoxide (CO) complex of hemoglobin in the *R* quaternary structure can be described to high precision by two linearly independent deoxyheme spectral components even though there is both tertiary relaxation and conversion to the *T* quaternary structure [35]. Furthermore, photodissociation of CO from the *T* quaternary structure shows spectral changes corresponding to tertiary conformational changes that are almost identical to those found in *R* [36]. Because of the presumed association of deoxyheme spectra with binding rates, these observations suggest that individual subunits exist in only two affinity states.

The present work is concerned with an initial exploration of the applicability of the TTS allosteric model to a subset of kinetic and equilibrium data. Only the time-resolved absorption spectra following nanosecond photodissociation of the CO complex of human hemoglobin are considered [35], as this remains the most complete set of data that measures the kinetics of both ligand rebinding and conformational changes over a wide range of times. Simultaneous fitting to the equilibrium CO binding curve and population of ligation states as a function of carbon monoxide saturation provides important constraints [37,38].

2. Methods

2.1. Kinetic rules

The set of tertiary states and notation for rates of the TTS model are shown in Fig. 2. As before [22], we have assumed that there is no coupling between protein conformation and the position of the ligand. The result of this assumption is that the rate of entry of the ligand into the protein to form the geminate state and the rate of exit of the ligand from the geminate state are independent of both tertiary and quaternary conformations, and, conversely, the rates of tertiary and quaternary conformational changes are independent of the position of the ligand. The observation of non-exponential tertiary relaxation processes has been attributed to incomplete equilibration of the conformational substates within a tertiary conformation on the time scale of interconversion between two overall tertiary conformations [39]. Rather than attempt to include the conformational substates explicitly, we have treated this effect approximately by introducing time dependence into the $r \rightleftharpoons t$ rate coefficients in order to produce a specified overall relaxation function [22]. The relaxation function chosen was the stretched exponential form $\exp[-(kt)^{\beta}]$, where $0 < \beta < 1$, with the same β for all tertiary rates. The method for simulating this relaxation in the model differential equations has been described in detail previously [22].

The rates of interconversion between a species in the *R* quaternary state and the corresponding *T*-state species with the same subunit states depend only on the tertiary states of the subunits and not the number of ligands bound per se. Because of the assumption that the subunits are indistinguishable, these rates depend only on the numbers of *r*- and *t*-state subunits in the tetramer. We designate

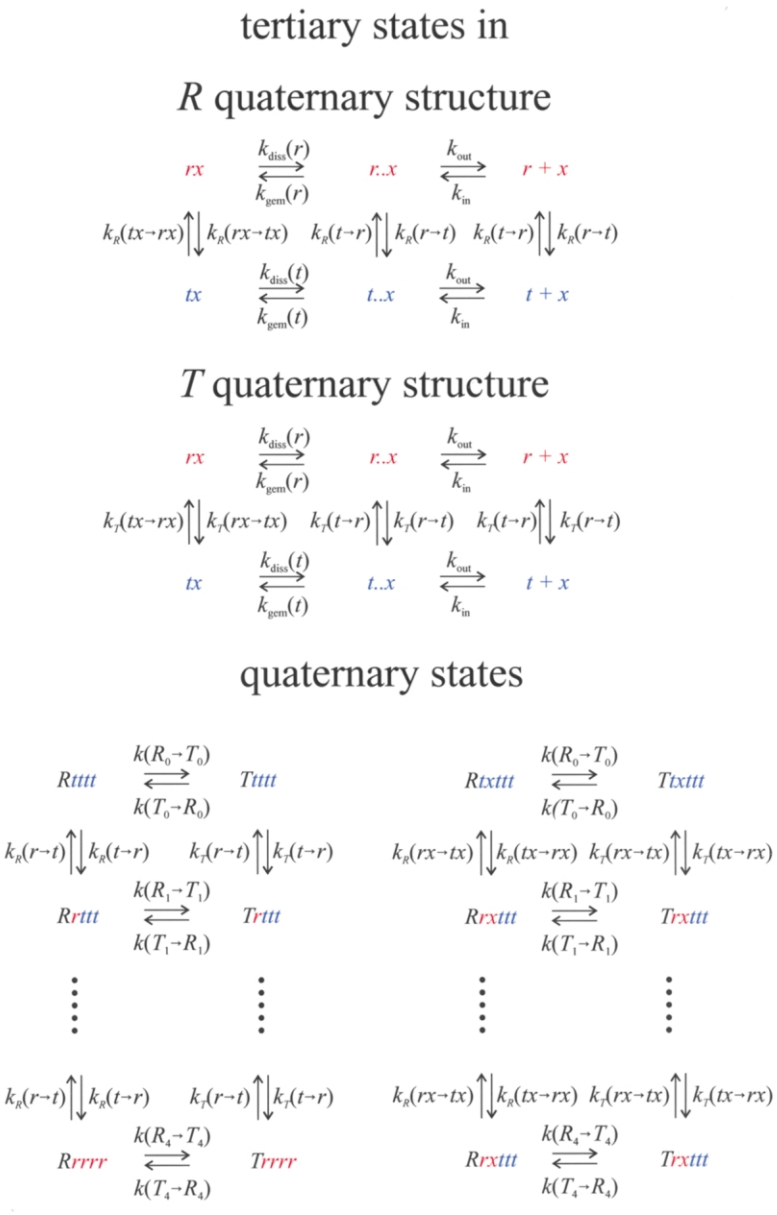

Fig. 2. States of the tertiary two-state model. Only a few quaternary states are shown, but they show that the quaternary rates depend only on the number of subunits in the *r* tertiary conformation, and not on the number of ligands bound as in the kinetic version of the QTS/MWC model of Henry et al. [22].

by $k(R_n \rightarrow T_n)$ and $k(T_n \rightarrow R_n)$ the quaternary rates for molecules containing n *r*-state subunits ($n = 0,1,2,3,4$). Rather than include all 10 rates as adjustable parameters, we assumed a linear free-energy relation between the quaternary rates and equilibrium constants [40] as a function of the number of *r*-state subunits in the tetramer, following a similar assumption made previously for rates and equilibrium constants indexed by numbers of bound ligands [22]. That is,

$$k(R_n \rightarrow T_n) = \gamma \left\{ \frac{L'}{l_R^4} \left(\frac{l_R}{l_T} \right)^n \right\}^{\alpha}$$

$$k(T_n \rightarrow R_n) = \gamma \left\{ \frac{L'}{l_R^4} \left(\frac{l_R}{l_T} \right)^n \right\}^{\alpha - 1}$$

where γ is a scaling parameter that sets the absolute rates, and $0 < \alpha < 1$. We could then choose a single reference $R \rightarrow T$ rate (i.e. for a single value of n) and derive all the other rates by scaling this rate up or down by powers of the scale factor $d = (l_R/l_T)^{-\alpha}$.

A complete enumeration of all possible combinations of tertiary/ligation states (selected from the set $\{r,r..x,rx,t,t..x,tx\}$) for the four subunits yields $6^4 = 1296$ combinations for each quaternary state. However, we have made the simplifying assumption that the subunits are indistinguishable (no $\alpha-\beta$ subunit inequivalence), yielding 126 tertiary/ligation configurations for each quaternary state, for a total of 252 species in the kinetic model. The model was implemented as a system of 252 differential equations describing the interconversions among these species. Allowed transitions between species with the same quaternary structure involve a change in the state of a single subunit. Stepwise changes in the subunit state take the form of either a change in the tertiary state or a change in the ligation state, but not both; ligation state changes were only permitted between the geminate state and either the unliganded state or the liganded state. Transitions involving a change in quaternary state were only permitted between species with identical tertiary/ligation configurations. With these restrictions a total of 2072 connections between kinetic species were enumerated for this model.

2.2. Computational methods

The application of the TTS model to sets of time-resolved spectra was similar to that described by Henry et al. [22] for the extended QTS model, and needs only be summarized here. The data used for the modeling consisted of difference spectra, spanning the wavelength range 390–470 nm, between equilibrium (unphotolyzed) HbCO and a photolyzed sample, measured at logarithmically spaced time intervals from nanoseconds to approximately 70 ms following photolysis by a 10-ns laser pulse. Sets of such spectra were measured for probe-pulse polarizations both parallel and perpendicular to the polarization of the photolysis pulse, and for 16 different levels of photolysis. Preliminary analysis of the data was described by Jones et al. [35] and results in sets of spectra, measured at n_p different photolysis levels, which are interpolated onto a single common grid of n_λ wavelengths and n_t time delays. These sets of spectra were collected into a single $n_\lambda \times (n_p n_t)$ data matrix **D**.

An essential simplification of the modeling was achieved by grouping the complete set of model species into n_s sets of spectroscopically distinct species, i.e. all species in a set were assumed to have the same spectrum. In our analysis, we assumed that the spectra of all subunits with a ligand bound to the heme (both unphotolyzed subunits and photolyzed subunits that have rebound ligands) are the same, and are proportional to the measured equilibrium spectrum of the HbCO tetramer; these subunits therefore do not contribute to the simulated difference spectra. Moreover, the spectra of all subunits without a bound ligand are distinguished only by the tertiary structure. Therefore, there are only $n_s = 2$ distinct spectra in the problem, the spectrum of unliganded r subunits and the spectrum of unliganded t subunits.

A single step in the modeling took the following form: for a given set of kinetic parameters, the system of differential equations describing the model was solved for each of the n_p initial sets of species populations derived from the different photolysis levels represented in the data. (For use in the modeling we selected $n_p = 5$ photolysis levels which span the range of the 16 levels represented in the full experimental data set.) This yielded for each photolysis level a set of populations of the 252 model species computed at each of the n_t experimental time delays, which were used to compute the time-dependent total populations of unliganded r subunits and unliganded t subunits. These populations comprised the $2 \times (n_p n_t)$ matrix **P**. The two corresponding unknown species spectra, of unliganded r subunits and unliganded t subunits, made up the columns

of the $n_\lambda \times 2$ matrix **S**, and were determined for a given population matrix **P** by solving the linear least-squares problem $\mathbf{SP} \approx \mathbf{D}$ [41].

The modeling was performed by adjusting the kinetic parameters to produce a matrix of time-dependent subunit populations **P** and a matrix of corresponding species spectra **S**, derived by least-squares, which together minimized the squared residual $\|\mathbf{D} - \mathbf{SP}\|^2$. Useful constraints on the parameters were imposed by introducing additional contributions to the overall residual to be minimized. For example, an optimal simulation of the experimental data was required not only to have a small residual matrix $\mathbf{D} - \mathbf{SP}$, but also to produce species spectra (columns of **S**) that are physically reasonable, as judged by the known shapes of such spectra. As before [22] it was found helpful in this regard to include a contribution to the residual given by the magnitude of the difference between the matrix of time- and photolysis-dependent populations of unrecombined deoxyhemes and the first amplitude vector (first column of the matrix **V**—see below) from the singular-value decomposition of the complete experimental data matrix **D**.

It was also required that the partition function derived from the kinetic parameters reproduce the observed equilibrium properties of CO binding to Hb. The equilibrium data used in this analysis were those of Perrella and co-workers [37,38] and consisted of a CO binding curve (saturation vs. CO pressure) and a set of populations of each of the five ligation states as a function of fractional saturation with CO. As before [22] we have allowed for differences in the values of selected parameters between the buffer used for these measurements (0.1 M chloride) and that used by Jones et al. (0.1 M phosphate). Since the sensitivity to solution conditions is primarily in the *T* quaternary structure, independent values for L' and l_T were used in fitting the equilibrium data, while the same values of the parameters K_t, K_r and l_R were used in fitting kinetic and equilibrium data.

Thus, the total residual to be minimized in the course of the modeling was given by the weighted sum of the residuals from simulation of the photolysis-dependent time-resolved spectra, from the comparison of the simulated ligand rebinding to the first SVD amplitude vector, and from simulation of the equilibrium CO binding data. A Marquardt–Levenberg algorithm was used to adjust the values of the various model parameters to effect this minimization, with constraints imposed to restrict the allowed range of certain parameters and parameter combinations (Tables 1 and 2).

3. Results

Fig. 3 shows the singular value decomposition (SVD) of the kinetic data of Jones et al. [35] on the photodissociation of the CO complex of human hemoglobin at room temperature. Five different levels of photolysis are shown. There are only two significant SVD components, indicating that all of the time-resolved spectra can be described by linear combinations of just two basis spectra (U_1 and U_2). This result also indicates that there are only two linearly independent liganded-minus-unliganded difference spectra. The basis spectrum of the dominant component (U_1) corresponds to the average spectrum and is very similar to a static liganded-minus-unliganded difference spectrum. The second basis spectrum (U_2) represents the deviation from the average spectrum, and describes the change in shape and amplitude of the deoxyheme photoproduct. The time course of the amplitude of U_1 (V_1) is an excellent approximation to the ligand rebinding curve, while the time course of the amplitude of the second basis spectrum (V_2) contains contributions from deoxyheme spectral changes caused by protein conformational changes, depletion of deoxyhemes by ligand rebinding, and spectral changes from kinetic hole burning.

The equilibrium data of Perrella and co-workers [37,38] are shown in Fig. 4. The data include the CO binding curve and the fraction of each ligation state as a function of fractional saturation with CO. Since we are not considering the effect of inequivalent binding to α and β subunits, the data for the individual species obtained by Perrella and DiCera [38] having the same number of ligands bound have been summed to give the results presented here for the five ligation states. In an MWC analysis of the data they found that the affinity of the *R* quaternary structure was the same for the two subunits, and that in the *T* quaternary

Table 1
Parameters of tertiary two-state model used in fitting to kinetic and equilibrium data

Parameter	Description	Fit value	Range of values[a]
L	Quaternary equilibrium constant $=[Tt_4]/[Rr_4]$	6×10^5	4×10^5–1×10^6
l_R	Tertiary equilibrium constant for deoxy subunits in R quaternary structure	0.7	0.5–0.8
l_T	Tertiary equilibrium constant for deoxy subunits in T quaternary structure	340	250–500
$k_R(r\rightarrow t)$	Tertiary transition rate for unliganded subunits in R quaternary structure	5.8×10^5 s^{-1}	2×10^5 to 1.5×10^6 s^{-1}
$k_T(r\rightarrow t)$	Tertiary transition rate for unliganded subunits in T quaternary structure	1×10^8 s^{-1}	$>10^8$ s^{-1}
$k_R(rx\rightarrow tx)$	Tertiary transition rate for liganded subunits in R quaternary structure	1 s^{-1}	0.1–10 s^{-1}
$k_T(rx\rightarrow tx)$	Tertiary transition rate for liganded subunits in T quaternary structure	90 s^{-1}	20–250 s^{-1}
$k_{gem}(r)$	Geminate rebinding rate to r	5.7×10^6 s^{-1}	$5\times10^6-7\times10^6$ s^{-1}
$k_{gem}(t)$	Geminate rebinding rate to t	7.6×10^3 s^{-1}	1×10^3 to 5×10^4 s^{-1}
k_{in}	Rate of ligand entry into the protein (Pseudo-first-order rate assumed independent of protein state)	2.4×10^4 s^{-1}	2.1×10^4 to 2.7×10^4 s^{-1}
k_{out}	Rate of ligand exit from protein (independent of protein state)	7.4×10^6 s^{-1}	6×10^6 to 9×10^6 s^{-1}
$k(R_3\rightarrow T_3)$	Quaternary rate, for tetramers containing three r subunits	5.7×10^3 s^{-1}	4×10^3 to 8×10^3 s^{-1}
d	Scale factor for $R\rightarrow T$ rates with decreasing number of r subunits	4.0	3–6
β	'Stretching' parameter for tertiary relaxation	0.6	0.5–0.7
K_r	Equilibrium constant for geminate binding to r subunits	3.6×10^8	2×10^8 to 5×10^8
K_t	Equilibrium constant for geminate binding to t subunits	1.1×10^5	10^4 to 10^6
L' (Cl^-)	L' for Cl^- solvent conditions of Perrella and co-workers [37,38]	9×10^5	2×10^5–4×10^6
l_T (Cl^-)	l_t for solvent conditions of Perrella and co-workers [37,38]	9×10^2	80 to 5×10^3

[a] This is the range of values obtained by varying one parameter at a time and noting the extremes at which the sum-of-squares increased by 20% above the value obtained at the minimum.

structure there was only a two-fold difference in affinity.

The model requires 16 independent parameters to fit the equilibrium and kinetic data. Five are required for the equilibrium data (Eq. (4)), and an additional 11 for the kinetic data. Because the equilibrium and kinetic data were collected under different solution conditions, the conformational equilibrium parameters of the model L' and l_T, but not l_R, were allowed to differ from those used in the kinetic fits. Table 1 gives the values of the parameters that were used in calculating the fitted curves in Figs. 3 and 4. Two additional constraints were employed in fitting the data. To be consistent with the approximately 10-fold difference in the two affinity states found in the gel equilibrium studies [34], more than approximately 90% of the liganded subunits in the T quaternary structure were required to be in the r tertiary conformation at equilibrium (by constraining $K_r/l_TK_t>10$). To insure the low geminate yield of the T state [36] the rate of the unliganded $r\rightarrow t$ tertiary conforma-

Table 2
Parameters derived from fit values required by detailed balance

$k_R(t \rightarrow r)$	9×10^5 s−1
$k_T(t \rightarrow r)$	3×10^5 s^{-1}
$k_R(tx \rightarrow rx)$	5×10^3 s^{-1}
$k_T(tx \rightarrow rx)$	9×10^2 s^{-1}
$k_{diss}(r)$	0.02 s^{-1}
$k_{diss}(t)$	0.07 s^{-1}
$k(R_0 \rightarrow T_0)$	4×10^5 s^{-1}
$k(R_1 \rightarrow T_1)$	9×10^4 s^{-1}
$k(R_2 \rightarrow T_2)$	2×10^4 s^{-1}
$k(R_4 \rightarrow T_4)$	1×10^3 s^{-1}
$k(T_0 \rightarrow R_0)$	0.1 s^{-1}
$k(T_1 \rightarrow R_1)$	10 s^{-1}
$k(T_2 \rightarrow R_2)$	2×10^3 s^{-1}
$k(T_3 \rightarrow R_3)$	2×10^5 s^{-1}
$k(T_4 \rightarrow R_4)$	3×10^7 s^{-1}

tional change in the T quaternary structure, $k_T(r \rightarrow t)$, was required to be greater than 10^8 s^{-1}.

A detailed picture of the kinetics can be obtained by showing populations of molecular species as a function of time (Fig. 5). The tertiary equilibrium constant for liganded subunits in R is 2×10^{-4}, so prior to photolysis only r is populated. Photodissociation results in unliganded r subunits which then either geminately rebind or relax to t. The geminate yield is primarily determined by a competition between ligand rebinding to r and ligand escape from the protein. Slow geminate rebinding by t has only a slight influence on determining the geminate yield because geminate rebinding is largely complete before the beginning of the stretched $r \rightarrow t$ tertiary conformational change which has a half-time of $\sim$1 μs. The kinetics now become complex because of the distribution of quaternary rates. The fastest $R \rightarrow T$ quaternary rate is for molecules that contain all t subunits. This rate $(=d^3\times k(R_3 \rightarrow T_3)=4^3\times5700)$ is 3.6×10^5 s^{-1}. The major contributor to the amplitude of deoxyheme spectral changes arising from quaternary conformational changes is for $R_2 \rightarrow T_2$, which takes place with a rate $(=d\times k(R_3 \rightarrow T_3))$ of 2.3×10^4 s^{-1}. This rate is much slower than the rate of 10^8 s^{-1} for $r \rightarrow t$ of unliganded subunits in T, so the tertiary change occurs instantaneously after the quaternary transition.

4. Discussion

4.1. Successes of the TTS model

Our objective in the present study was to determine whether a kinetic version of the tertiary two-state (TTS) allosteric model could fit the extensive kinetic data of Jones et al. [35], and also be consistent with equilibrium data on solutions, gels and crystals. Figs. 3 and 4 show the kinetic and equilibrium data, together with the fits obtained by the TTS allosteric model, with parameters summarized in Table 1. The previous fit to the

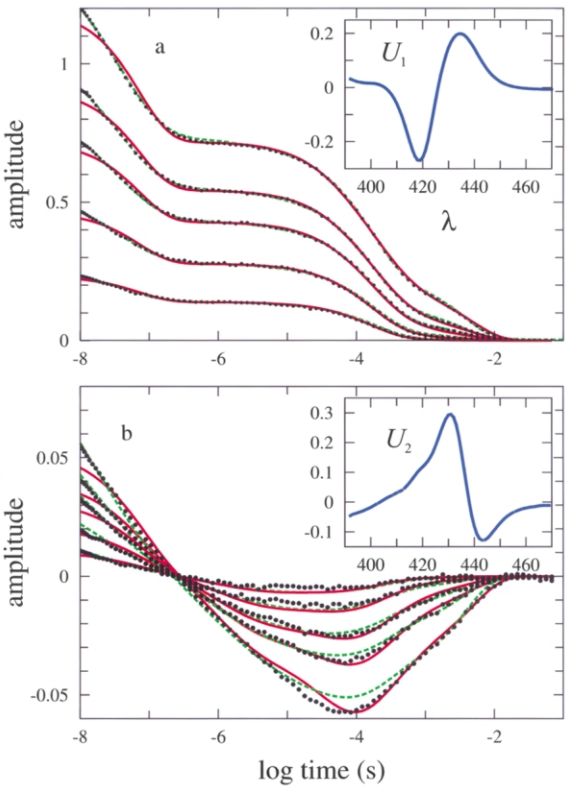

Fig. 3. Kinetic data and fits with TTS and extended QTS models. (a) kinetics of ligand rebinding. (b) Kinetics of conformational changes of deoxyheme photoproduct. In both panels the points are the experimental data, the (green) dashed curves are the fits from Henry et al. [22] using the extended QTS model of MWC, and the (red) continuous curves are the fits from the TTS model using the parameters given in Table 1. The fit to the ligand rebinding with the QTS/MWC model is so good that the dashed curves are barely visible.

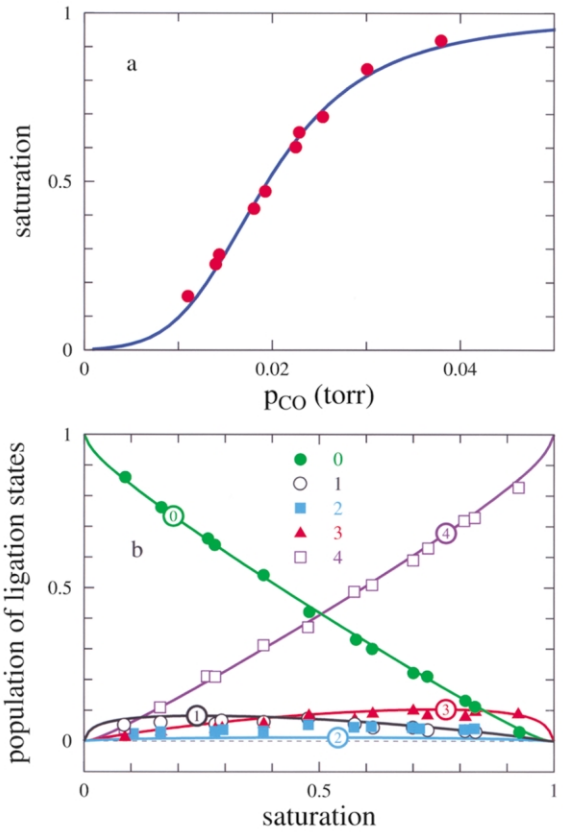

Fig. 4. Equilibrium data of Perrella and co-workers [37,38] and fits with TTS model. (a) Equilibrium CO binding curve. The (blue) continuous curve is the fit with the TTS model using the parameters in Table 1. (b) Equilibrium population of ligation states as a function of saturation. The continuous curves are the fit to the data using the parameters in Table 1: zero-liganded (filled circles), singly-liganded (open circles), doubly-liganded (filled-squares), triply-liganded (filled triangles), quadruply-liganded (open squares).

kinetic data using an extension of the quaternary two-state (QTS) model of MWC [22] is shown for comparison. Except for the first 30 ns, the fit to the kinetic data is superior to what was found previously with the extended QTS/MWC model. Although 16 parameters were varied in the kinetic modeling, each parameter has a well-defined physical interpretation. Furthermore, the number of model parameters is much lower than the 30–67 parameters (amplitudes and relaxation times) that are required for a purely empirical description of the kinetic data [22]. The remaining 15 parameters of the model result from detailed balance (Table 2). The fits to the CO saturation curve and the fraction of ligation states as a function of CO saturation are most probably within the experimental errors of these measurements, with the possible exception of the fraction of doubly-liganded species (see below).

In the extended QTS/MWC model, the disappearance of the immediate product of photolysis, labeled r^*, was postulated to explain the time course at the earliest times. The stretched tertiary conformational change from r^* to r (within R), with a corresponding decrease in geminate rebinding rate, explained the non-exponential geminate rebinding. In the TTS model the stretched tertiary conformational change from r to t in the R quaternary structure occurs at times ($t_{1/2} \approx 1$ μs) longer than the tertiary conformational change of the extended QTS/MWC model ($t_{1/2} \approx 60$ ns) [22]. It therefore has relatively little effect on the geminate process, and accounts for the more exponential-like geminate rebinding phase of the TTS model (Fig. 3). The TTS model does not distinguish between liganded and unliganded subunits in the high affinity r conformation, so it appears that it is somewhat of an oversimplification as far as the geminate kinetics are concerned.

Perhaps the most interesting parameters of the model are the tertiary conformational equilibrium constants in R and T for liganded and unliganded subunits (l_R and l_T). They predict that in the R quaternary structure at equilibrium liganded subunits are all in the r tertiary conformation and in the T quaternary structure all unliganded subunits are in the t tertiary conformation. The incomplete coupling of tertiary and quaternary structure is revealed in unliganded R and liganded T. The occupancy of the t conformation for unliganded subunits in R is 40%, while the occupancy of the r conformation for liganded subunits in T is 90%. This latter value could be smaller, because the minimization was constrained to have 90% as the lowest allowed occupancy. The purpose of the constraint was to determine whether it is possible to provide a quantitative explanation of the kinetic data with parameters that are consistent with one of the major results of recent binding studies of hemoglobin encapsulated in silica gels [34]. Like

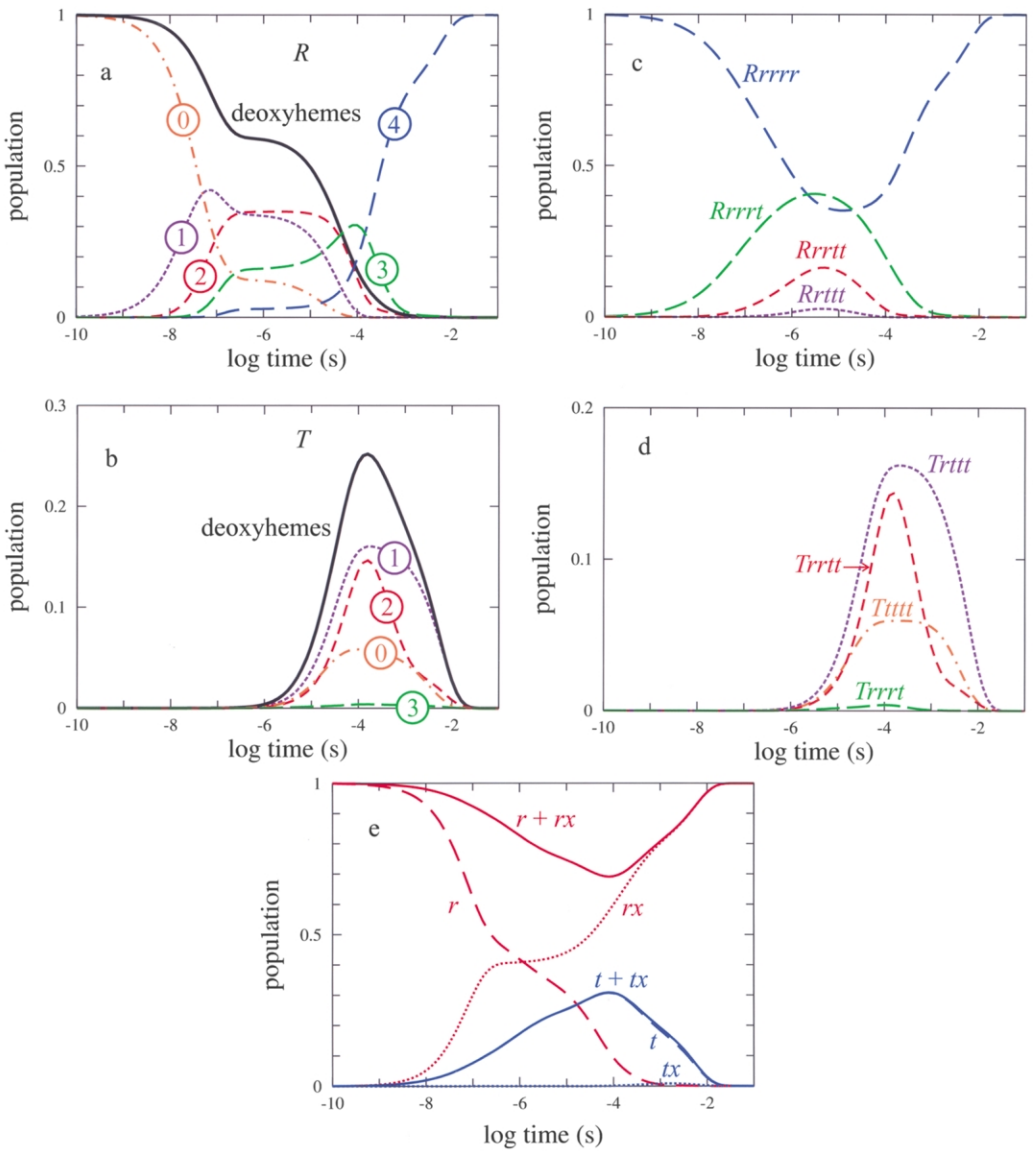

Fig. 5. Time course of populations of subunit and quaternary conformational states predicted by TTS model following 100% photolysis using the parameters of Table 1. (a) Population of tetramers containing various number of ligands in the *R* quaternary structure (dashed curves); deoxyheme population in *R* quaternary structure (continuous curve). (b) Population of tetramers containing various numbers of ligands in the *T* quaternary structure (dashed curves); deoxyheme population in *T* quaternary structure (continuous curve). The population of *T*-state tetramers with four ligands bound is too small to be observable on a linear scale. (c) Population of tetramers containing various numbers of subunits in the *r* (the sum of liganded and unliganded) tertiary conformation in the *R* quaternary structure. The population of *R*-state tetramers with all subunits in the *t* (*Rtttt*) conformation is too small to be observable on a linear scale. (d) Population of tetramers containing various numbers of subunits in the *r* conformation in the *T* quaternary structure. The population of *T*-state tetramers with all subunits in the *r* (*Trrrr*) conformation is too small to be observable on a linear scale. (e) Populations of subunits in the *r* and the *t* tertiary conformations: total *r* and total *t* (continuous curves), deoxy (dashed) and liganded (dotted) *r* and *t* (dashed curves). Notice that almost all of the subunits in the *t* conformation are unliganded.

the crystal, the gel enormously slows the quaternary conformational change as determined by oxygen binding measurements. Gels prepared in the absence of oxygen remain in the *T* quaternary structure upon oxygenation and only slowly convert to *R*. Bruno et al. [34] found that encapsulation in the presence of the strong allosteric effectors inositol hexaphosphate and bezafibrate produces a non-cooperative binding curve (Hill $n = 0.94 \pm 0.02$) with an affinity 10-fold lower than for deoxyhemoglobin encapsulated in the absence of these effectors (Hill $n = 0.93 \pm 0.03$). (The Hill *n* values lower than 1.0 were explained by Bruno et al. as arising from inequivalence of the affinities of α and β subunits.) In the presence of allosteric effectors the affinity was found to be very close to that determined in single crystal studies and, as in the crystal, independent of pH. Bruno et al. interpreted their results as evidence for the existence of two tertiary conformations within the *T* state, as was proposed by Rivetti et al. [17]. A similar interpretation has been given by Shibayama and Saigo [33], except that they found a larger difference between the high and low affinity states.

In the context of the present model, binding to the crystal or the low affinity gel state would correspond to binding by *t* in the *T* quaternary structure with no change in tertiary (or quaternary) conformation. In contrast, the 10-fold higher affinity state of the gel without allosteric effectors would correspond to binding of a ligand to *t* followed by a tertiary conformational change from *tx* to *rx* (but no *T* to *R* quaternary change) with an approximately 1:10 population ratio (Eq. (5), Fig. 2). In gels where both states are present [32,33], one would argue that the multiphasic binding curve results from the gel kinetically constraining molecules from making the $tx \rightarrow rx$ conformational change within *T*.

Another interesting consequence of the model is that it predicts the spectral changes following photolysis of carbonmonoxyhemoglobin, initially in the *T* quaternary structure, to have the same shape as those observed for photolysis of the liganded R structure, since they both should reflect the unliganded *r* to *t* conformational change. These changes were most clearly seen in a study of an iron/cobalt hybrid hemoglobin with cobalt substituted for iron in the β subunits [36]. Since the cobalt heme does not bind CO, the fully saturated molecule contains only two ligands and could be converted to more than 90% *T* with inositol hexaphosphate and bezafibrate, as judged by the markedly decreased geminate yield, absence of any conformational changes in the 10-μs relaxation, and mostly slow bimolecular rebinding [36]. The shape of the spectral change for the tertiary relaxation following photodissociation is nearly identical, although slightly blue-shifted, to that found in the absence of allosteric effectors where it is presumed that the molecule is almost entirely in the *R* quaternary structure.

4.2. Problems with the TTS model

One problem with the TTS model is that it is apparently inconsistent with the observation in photodissociation studies of tertiary conformational changes taking place at times longer than 10 ns for hemoglobin initially in the *T* quaternary structure [36,42]. Murray et al. [36] found the tertiary relaxation times following photodissociation of *R* and *T*-state iron/cobalt hybrids to be very similar. In order to have a high population of liganded *r* conformations in the *T* quaternary structure, but simultaneously account for the low geminate yield of the *T* state, it is necessary for the $r \rightarrow t$ rate in *T* to be sufficiently fast that it is nearly complete before the beginning of geminate rebinding. This leaves the apparent $r \rightarrow t$ conformational change, described by relaxations at 40 and 330 ns [36], unexplained. One possible way of rationalizing this result, as well as the inability of the model to fit the data in Fig. 3 for the first ~ 30 ns, is to consider the distribution of conformational substates, as first described for myoglobin [43]. Hagen et al. [44,45] showed that for myoglobin embedded in a trehalose glass at room temperature, the rates of geminate rebinding for individual conformational substates vary by more than a factor of 10^6. The observation of a stretched exponential time course for the tertiary conformational change in myoglobin has been interpreted using a model in which interconversion of conformational substates occurs on the same time scale as the overall conformation change [39]. The tertiary relaxation

in both *R* and *T* states is also a stretched exponential [22,35,36]. If substate interconversion is comparable to or slower than the ~100 ns required to complete the geminate rebinding phase, then the distribution of substates and the rates of substate interconversion should be considered for an accurate description of the kinetics. In this more detailed description, one might imagine that it is still possible to have well-defined *r* and *t* states for explaining equilibrium data or kinetic data at times longer than ~1 μs, when substate interconversion is sufficiently rapid that the equilibrium distribution is maintained. For example, in the fully liganded *T* quaternary structure, where 90% of the subunits (with the current parameters) are in the *r* conformation, one could imagine that the *T* quaternary structure biases the distribution of substates toward conformations that are more *t*-like. This could simultaneously account for the low geminate yield of the *T* state, and an $r \rightarrow t$ conformational change that occurs during and after the completion of geminate rebinding. The deviations of the fit with the TTS model at early times in Fig. 3 might also be explained by such considerations. Moreover, the small differences between the deoxyheme spectral changes associated with the tertiary relaxations in *T* and *R* in the iron/cobalt hybrids are consistent with these ideas.

Another problem with the TTS model is that it is not capable of accurately predicting the population of doubly liganded species from low temperature electrophoresis experiments reported by Perrella and Di Cera [38] (Fig. 4b). As these authors and Ackers [15] have pointed out, there is no simple way of rationalizing the distribution of the four distinct doubly-liganded states. Introducing inequivalence of α and β subunits and cooperativity within the αβ dimer (i.e. the interaction found by Ackers [15] and described by the dimeric cooperon model) does not eliminate the discrepancy with either the TTS model or the QTS/MWC model.

Finally, we should point out that Gibson [46] has revisited the problem of the kinetics of oxygen binding and concluded that the MWC model cannot simultaneously explain the data on metal hybrids and the unsubstituted tetramer. It will be interesting to determine whether this apparent discrepancy can be resolved by the TTS model.

4.3. Concluding remarks

We have shown that it is possible for a tertiary two-state (TTS) model to fit a demanding set of kinetic data reasonably well with parameters that are consistent with the equilibrium results from solution, crystal and gel binding studies. This model has the same spirit as the original MWC model in that there are only two affinity states and non-cooperative binding within each quaternary structure. There is, however, inconsistency with the low temperature electrophoresis data that remains to be resolved. Although we have not discussed the subject in any detail, the model provides a natural way of exploring the influence of allosteric effectors [27,47], and this would be an important next step. It would also be interesting to reinvestigate the X-ray crystallographic structures of unliganded hemoglobin in the *R* quaternary structure and liganded hemoglobin in the *T* quaternary structure, with the view of describing the data in terms of a mixture of *r* and *t* conformations.

Acknowledgments

We thank Andrea Mozzarelli and Attila Szabo for many helpful discussions. S.B. thanks EMBO for a long-term fellowship.

References

[1] J. Monod, J. Wyman, J-P. Changeux, On the nature of allosteric transitions: a plausible model, J. Mol. Biol. 12 (1965) 88–118.
[2] M. Brunori, Hemoglobin is an honorary enzyme, Trends Biochem. Sci. 24 (1999) 158–161.
[3] M.F. Perutz, Stereochemistry of cooperative effects in haemoglobin, Nature 228 (1970) 726–739.
[4] E. Antonini, M. Brunori, Hemoglobin and Myoglobin in their Reactions with Ligands, North-Holland Publishing Co, Amsterdam, 1971.
[5] A. Szabo, M. Karplus, A mathematical model for structure-function relations in hemoglobin, J. Mol. Biol. 72 (1972) 163–197.
[6] J. Herzfeld, H.E. Stanley, A general approach to cooperativity and its application to the oxygen equilibrium of hemoglobin and its effectors, J. Mol. Biol. 82 (1974) 231–265.

[7] R.G. Shulman, J.J. Hopfield, S. Ogawa, Allosteric interpretation of haemoglobin properties, Q. Rev. Biophys. 8 (1975) 325–420.
[8] S.J. Edelstein, Cooperative interactions of hemoglobin, Annu. Rev. Biochem. 44 (1975) 209–232.
[9] M.F. Perutz, A.J. Wilkinson, M. Paoli, G.G. Dodson, The stereochemistry of the cooperative effects in hemoglobin revisited, Annu. Rev. Biophys. Biomol. Struct. 27 (1998) 1–34.
[10] W.A. Eaton, E.R. Henry, J. Hofrichter, A. Mozzarelli, Is cooperative oxygen binding by hemoglobin really understood?, Nat. Struct. Biol. 6 (1999) 351–358.
[11] R.G. Shulman, Spectroscopic contributions to the understanding of hemoglobin function: implications for structural biology, IUBMB Life 51 (2001) 351–357.
[12] J.-P. Changeux, S.J. Edelstein, Allosteric receptors after 30 years, Neuron 21 (1998) 959–980.
[13] M. Brunori, M. Coletta, E. Di Cera, A cooperative model for ligand-binding to biological macromolecules as applied to oxygen carriers, Biophys. Chem. 23 (1986) 215–222.
[14] S.J. Gill, C.H. Robert, M. Coletta, E. DiCera, M. Brunori, Cooperative free energies for nested allosteric models as applied to human hemoglobin, Biophys. J. 50 (1986) 747–752.
[15] G.K. Ackers, Deciphering the molecular code of hemoglobin allostery, Adv. Protein Chem. 51 (1998) 185–253.
[16] A. Mozzarelli, C. Rivetti, G.L. Rossi, E.R. Henry, W.A. Eaton, Crystals of haemoglobin with the T quaternary structure bind oxygen non-cooperatively with no Bohr effect, Nature 351 (1991) 416–418.
[17] C. Rivetti, A. Mozzarelli, G.L. Rossi, E.R. Henry, W.A. Eaton, Oxygen binding by single crystals of hemoglobin, Biochemistry 32 (1993) 2888–2906.
[18] A. Mozzarelli, C. Rivetti, G.L. Rossi, W.A. Eaton, E.R. Henry, Allosteric effectors do not alter the oxygen affinity of hemoglobin crystals, Protein Sci. 6 (1997) 484–489.
[19] L. Kliger, M.C. Marden, Asymmetric [deoxy dimer/azido-met dimer] hemoglobin hybrid tetramers dissociate within seconds, J. Mol. Biol. 291 (1999) 227–236.
[20] J.J. Hopfield, R.G. Shulman, S. Ogawa, An allosteric model of hemoglobin: I, kinetics, J. Mol. Biol. 61 (1971) 425–443.
[21] C.A. Sawicki, Q.H. Gibson, Quaternary conformational changes in human hemoglobin studied by laser photolysis of carboxyhemoglobin, J. Biol. Chem. 251 (1976) 1533–1542.
[22] E.R. Henry, C.M. Jones, J. Hofrichter, W.A. Eaton, Can a two-state MWC allosteric model explain hemoglobin kinetics?, Biochemistry 36 (1997) 6511–6528.
[23] M.F. Perutz, L.F. TenEyck, Stereochemistry of cooperative effects in hemoglobin, Cold Spring Harbor Symp. Quant. Biol. 36 (1971) 569.
[24] M.W. Makinen, W.A. Eaton, Optically detected conformational changes in haemoglobin single crystals, Nature 247 (1974) 62–64.
[25] A.P. Minton, K. Imai, The three-state model: a minimal allosteric description of homotropic and heterotropic effects in the binding of ligands to hemoglobin, Proc. Natl. Acad. Sci. USA 71 (1972) 1418–1421.
[26] K. Imai, Allosteric Effects in Hemoglobin, Cambridge University Press, Cambridge, 1982.
[27] K. Imai, The Monod–Wyman–Changeux allosteric model describes haemoglobin oxygenation with only one adjustable parameter, J. Mol. Biol. 167 (1983) 741–749.
[28] A. Lee, M. Karplus, C. Poyart, E. Bursaux, Analysis of proton release in oxygen binding by hemoglobin-implications for the cooperative mechanism, Biochemistry 27 (1988) 1285–1301.
[29] L. Pauling, The oxygen equilibrium of hemoglobin and its structural interpretation, Proc. Natl. Acad. Sci. USA 21 (1935) 186–191.
[30] D.E. Koshland, G. Nemethy, D. Filmer, Comparison of experimental binding data and theoretical models in proteins containing subunits, Biochemistry 5 (1966) 365–385.
[31] N. Shibayama, S. Saigo, Fixation of the quaternary structures of human adult haemoglobin by encapsulation in transparent porous silica gels, J. Mol. Biol. 251 (1995) 203–209.
[32] S. Bettati, A. Mozzarelli, T state hemoglobin binds oxygen noncooperatively with allosteric effects of protons, inositol hexaphosphate, and chloride, J. Biol. Chem. 272 (1997) 32050–32055.
[33] N. Shibayama, S. Saigo, Direct observation of two distinct affinity conformations in the T state human deoxyhemoglobin, FEBS Lett. 492 (2001) 50–53.
[34] S. Bruno, M. Bonaccio, S. Bettati, et al., High and low oxygen affinity conformations of T state hemoglobin, Protein Sci. 10 (2001) 2401–2407.
[35] C.M. Jones, A. Ansari, E.R. Henry, G.W. Christoph, J. Hofrichter, W.A. Eaton, The speed of intersubunit communication in proteins, Biochemistry 31 (1992) 6692–6702.
[36] L.P. Murray, J. Hofrichter, E.R. Henry, et al., The effect of quaternary structure on the kinetics of conformational changes and nanosecond geminate rebinding of carbon monoxide to hemoglobin, Proc. Natl. Acad. Sci. USA 85 (1988) 2151–2155.
[37] M. Perrella, A. Colosimo, L. Benazzi, M. Ripamonti, L. Rossi-Bernardi, What the intermediate compounds in ligand binding to hemoglobin tell about the mechanism of cooperativity, Biophys. Chem. 37 (1990) 211–223.
[38] M. Perrella, E. Di Cera, CO ligation intermediates and the mechanism of hemoglobin cooperativity, J. Biol. Chem. 274 (1999) 2605–2608.

[39] S.J. Hagen, W.A. Eaton, Nonexponential structural relaxations in proteins, J. Chem. Phys. 104 (1996) 3395–3398.
[40] W.A. Eaton, E.R. Henry, J. Hofrichter, Application of linear free energy relations to protein conformational changes: the quaternary structural change of hemoglobin, Proc. Natl. Acad. Sci. USA 88 (1991) 4472–4475.
[41] E.R. Henry, The use of matrix methods in the modeling of spectroscopic data sets, Biophys. J. 72 (1997) 652–673.
[42] J. Hofrichter, J.H. Sommer, E.R. Henry, W.A. Eaton, Nanosecond absorption spectroscopy of hemoglobin, elementary processes in kinetic cooperativity, Proc. Natl. Acad Sci. USA 80 (1983) 2235–2239.
[43] R.H. Austin, K.W. Beeson, L. Eisenstein, L.H. Frauenfelder, I.C. Gunsalus, Dynamics of ligand binding to myoglobin, Biochemistry 14 (1975) 5355–5373.
[44] S.J. Hagen, J. Hofrichter, W.A. Eaton, Protein reaction kinetics in a room-temperature glass, Science 269 (1995) 959–962.
[45] S.J. Hagen, J. Hofrichter, W.A. Eaton, Geminate rebinding and conformational dynamics of myoglobin embedded in a glass at room temperature, J. Phys. Chem. 100 (1996) 12008–12021.
[46] Q.H. Gibson, Kinetics of oxygen binding to hemoglobin A, Biochemistry 38 (1999) 5191–5199.
[47] T. Yonetani, A. Tsuneshige, The oxygen affinity of hemoglobin is modulated primarily by heterotropic tertiary constraints rather than the T/R quaternary structural changes, Biophys. J. 80 (2001) 1176.
[48] R.E. Dickerson, I. Geis, Hemoglobin: Structure, Function, Evolution, and Pathology, Benjamin/Cummings, Menlo Park, CA, 1983.